

# Spectrally-Pure Optical Serrodyne Modulation for Continuously-Tunable Laser Offset Locking

Roame A. Hildebrand<sup>1,2</sup>, Alessandro Restelli<sup>4</sup>, Wance Wang<sup>1,2</sup>, Connor Goham<sup>1,2</sup>, and Joseph W. Britton<sup>2,3</sup>

<sup>1</sup>*Institute for Research in Electronics and Applied Physics, University of Maryland, College Park, MD 20742, USA*

<sup>2</sup>*Department of Physics, University of Maryland, College Park, MD 20742, USA*

<sup>3</sup>*U.S. Army Combat Capabilities Development Command, Army Research Laboratory, Adelphi, MD 20783, USA*

<sup>4</sup>*Joint Quantum Institute, University of Maryland and the National Institute of Standards and Technology, College Park, MD 20742, USA*

## Abstract

The comb-like spectrum added to laser light by an electro-optic modulator (EOM) finds use in a wide range of applications including coherent optical communication [1], laser frequency and phase stabilization [2], and atomic spectroscopy [3]. In some cases a sideband-free optical frequency shift is preferred, such as in laser-offset locking using an optical cavity [4], single-photon frequency shifting [5], and laser range finding [6, 7]. Approaches to obtaining an optical frequency offset (OFO) involve trade-offs between shift range, conversion gain, and suppression of spurious sidebands. Here we demonstrate an OFO of continuous-wave laser light by serrodyne modulation using a fiber EOM and radio-frequency (RF) tones from a commodity RF system on a chip (RFSoc) to achieve shifts of 40 to 800 MHz with  $> 15$  dB suppression of spurious sidebands and  $< 1.5$  dB conversion loss. We also observe smoothly-varying conversion gain. The utility of this tool is demonstrated by continuously shifting the offset of a cavity-locked laser from 50 to 1600 MHz, a capability useful in spectroscopy of unknown optical transitions.

The performance requirements for OFO depends on application. Continuously-tunable Pound-Drever-Hall (PDH) laser-offset locks are simplified by spectrally-pure shifts covering ranges greater than half the cavity free spectral range (FSR) and sufficient power stability in the shifted sideband to maintain lock across the sweep bandwidth. Whereas for single-photon frequency shifting, low insertion loss, high conversion efficiency and precise frequency control is desirable to maximize interference visibility [5]. The resolution of laser range finding is limited by optical frequency chirp nonlinearity [6, 7], favoring an OFO with high bandwidth and precise frequency control. We expect a wide range of applications will benefit from improved OFO tools.

Here we show that commodity arbitrary waveform generators and waveguide electro-optic modulators enable substantially improved OFO performance for continuous-wave laser light relative to prior demonstrations. We characterize the shift quality via two measures: conversion loss and suppression. Let  $P_{\text{in}}$  be the power in the optical fiber upstream of the EOM and  $P_{\text{out}}$  be the power out of the EOM with

no RF applied. Conversion loss is defined as the ratio  $\beta = P_{\text{out}}/P_{\text{shift}}$  and suppression as the ratio  $\gamma = P_{\text{shift}}/P_{\text{spur}}$ , where  $P_{\text{shift}}$  is power at the target frequency in the output spectrum and  $P_{\text{spur}}$  is the maximum power at any frequency that is not the target frequency in the output spectrum. We also define insertion loss  $\alpha = P_{\text{in}}/P_{\text{out}}$ .

The most straight-forward and flexible method to obtain light at a frequency offset is beat-note locking a pair of independent lasers. This approach admits a wide tuning range, fast frequency shifting (limited by laser lock bandwidth), high optical power, and zero sidebands, but requires the use of a second laser. The most general but expensive approach is offsetting a pair of lasers via locking to an optical frequency comb. Free-space acousto-optic modulators (AOMs) rely on phonon scattering and permit single-pass shifts of 80 MHz to 500 MHz, high optical power handling, and excellent carrier suppression, but suffer from low tuning bandwidth ( $< 50\%$ ), moderate insertion loss ( $\sim 1$  dB) and a frequency-dependent angular shift. Multi-pass AOM setups [8] permit a greater absolute shift and remedy the frequency-dependent an-

gular shift but have limited tuning bandwidth, high insertion loss (e.g. 5 GHz  $\pm$  150 MHz,  $-10$  dB [9]) and are challenging to keep aligned. Electro-optic phase modulators (EOMs) rely on the electro-optic effect to mix optical and microwave signals. They are an attractive option for larger frequency shifts with the added complexity of polarization sensitivity. Free-space EOMs offer high optical power handling but often rely on high-quality-factor resonators to obtain the necessary RF voltage, which constrains the RF bandwidth [10]. Waveguide-based EOMs have greater bandwidth ( $\sim 50$  GHz) and high modulation efficiency but low optical power handling.

There are several EOM-based approaches to OFO. A single optical sideband can be obtained from interference of EOM-generated in-phase and in-quadrature (IQ) optical fields, but the minimum conversion loss is 4.7 dB and the technical overhead is high [1, 11, 12]. For example, Kawanishi *et al.* used 4 EOMs, 4 DC biases and 4 RF drives to obtain shifts of  $\pm 40$  GHz with 6.9 dB insertion loss and 17 dB suppression. In 2021, the Loncar group used a pair of evanescently coupled lithium-niobate ring resonators driven by an RF tone to implement on-chip OFO with a conversion loss of  $< 1.2$  dB from 8 GHz to 11 GHz [13]. This novel approach may be the future of OFO in highly integrated devices, but is not yet commercially available.

Serrodyne modulation is an alternative approach that applies a quasi-continuous optical phase ramp to generate an OFO. A voltage  $V(t)$  applied across the electro-optic material shifts the optical phase:  $E_0 \sin(2\pi\xi t + \phi(t))$ , where  $\xi$  is the input optical frequency and  $\phi(t) = \frac{\pi}{V_\pi} V(t)$ . For serrodyne modulation the voltage waveform is a sawtooth

$$V_s(t) = 2NV_\pi \left[ (f_m t \bmod 1) - \frac{1}{2} \right] \quad (1)$$

with frequency  $f_m$  and peak-to-peak amplitude  $2NV_\pi$  for  $N \in \mathbb{N}$ . The idealized EOM output is then  $(-1)^N E_0 \sin[2\pi(\nu + Nf_m)t]$ , effectively shifting the laser frequency by  $Nf_m$ . In practice, the output has unwanted spectral features due to imperfections in  $V_s(t)$ , improper impedance matching to the electro-optic medium, and RF amplifier finite bandwidth and frequency-dependent gain.

An early effort by Johnson and Cox (1988) obtained a serrodyne shift of 5 kHz using a voltage ramp produced by charging a capacitor [14]. A later innovation exploited the extreme nonlinearity of commercially-available nonlinear transmission lines (NLTL) [15, 16]. For example, the Kasevich group obtained a conversion loss of 1.0 dB at 1.5 GHz shift, 10 dB suppression over 940 to 1200 MHz, and

7 dB suppression over 200 to 1240 MHz [16]. Wide bandwidth OFO proved challenging with NLTLs despite experimentation with a range of devices. All-optical serrodyne modulation was demonstrated using cross-phase modulation in a nonlinear fiber but has high technical overhead and small bandwidth [17]. Recently, modern arbitrary waveform generators (AWG) have enabled improved sawtooth waveforms at low cost. Minjeong Kim *et al.* obtained conversion losses as low as 0.13 dB over tens of megahertz, but did not attempt modulations beyond 400 MHz [18]. Table 1 compares the range of approaches discussed so far.

Here we show that the use of low-cost, high-bandwidth AWGs permits substantial improvement in high bandwidth OFO using off-the-shelf components. In this scheme, an AWG provides the voltage ramp, which is then amplified and applied to a fiber EOM. We demonstrate the utility of our OFO by using it to continuously tune the offset of an 870 nm laser from an optical cavity mode by 50 MHz to 1600 MHz. We also model the consequence of poor RF spur suppression when continuously tuning Pound Dreyer Hall (PDH) offset locks.

## 1 Apparatus

The optical elements of our apparatus consist of a laser, fiber polarization paddles, a fiber EOM, and an optical spectrum analyzer. The single-mode laser is an 870 nm ECDL (Toptica DLC Pro). The EOM is a LiNbO3 phase modulator with 3.3 dB insertion loss, 27 dBm max RF input power,  $V_\pi = 1.6$  V (measured at 1 GHz), and an electro-optic modulation response that varies by up to 3 dB over DC to 14 GHz (EOSPACE PM-0S5-10-PFA-PFA-800-P5). The EOM is packaged with FC/APC connectors and Panda-type polarization maintaining (PM) fiber. We used polarization paddles ( $\lambda/4$ ,  $\lambda/2$ ,  $\lambda/4$ ) to align the polarization with the EOM modulation axis and obtain an average polarization extinction ratio (PER) of 23.5 dB at the input of the EOM fiber.

The optical spectrum analyzer is a scanning Fabry-Pérot interferometer (FPI) with  $\sim 7.5$  MHz resolution and 3 GHz free spectral range (FSR; Thorlabs SA200-8B). We measure an optical power spectrum by scanning the FPI cavity length across the cavity FSR while monitoring transmission on a photodetector. We confirmed that we are operating the FPI photodetector in the linear regime. Our measurements are insensitive to nonlinearity and hysteresis in the FPI PZT as we are only measuring cavity transmission of discrete spectral features, not their relative

positions. We only explored OFO  $> 40$  MHz due to limited FPI resolution.

The RF serrodyne signal is generated by an AWG followed by an amplifier, which then drives the EOM. The AWG is a commodity RFSoc (AMD Xilinx RFSoC 4x2), a development board based on the AMD ZYNQ Ultrascale+ RFSoc ZU48DR device. The AMD device is a monolithic radio-frequency system on chip (RFSoc) that contains a processing system (PS) with a quad-core 64-bit ARM processor and a dual-core 32-bit ARM, a field programmable gate array (FPGA) with nearly a million programmable logic cells (PL), and eight 14-bit digital to analog converters (DAC) with a maximum sampling rate of 10 GSPS. The RFSoc 4x2 development board exposes only 4 ADC channels and 2 DAC channels to the user. We wrote in Verilog a ramp generator core based on a 32-bit accumulator with 32-bit programmable increment  $inc$  to feed one of the RFSoC DAC channels with a digital ramp. Since the SoC PL cannot work at the 10 GHz rate of the DAC channel, we enabled multiplexing in the DAC and the ramp generator core is run at a clock frequency of 615 MHz and replicated 16 times to calculate 16 output samples for each PL clock cycle. The resulting 32-bit registers are multiplied by a 16-bit gain factor  $g$  and the 14 most significant bits of the 16 48-bit results are fed to the DAC core during each PL clock cycle resulting in a 9.85 GSPS analog output. The programmable increment  $inc$  and gain  $g$  are memory mapped to the PS system memory using automatically generated cores available in AMD Vivado. The PS runs PYNQ (Python Productivity for ZYNQ), a Linux Ubuntu-based distribution, and allows the user to write Python application programming interfaces (API) to interface PL and PS through memory mapped registers or direct memory access (DMA). In our specific case we wrote an API to adjust amplitude and frequency of the sawtooth waveform. The Python code also manages the conversion between physical units (normalized scaling factor and Hz) and hardware units (16 and 32-bit codes) used in  $g$  and  $inc$  registers. The latency for changing the shift frequency via python executed on the board in the current unoptimized implementation is  $\sim 75 \mu\text{s}$ —the minimum possible latency is 40 ns set by the DAC pipeline. The source for the ramp generator is available on GitHub. The RF amplifier has a bandwidth of 10 to 4200 MHz, 37 dB gain varying by at most 1.5 dB over its bandwidth, +32 dBm P1dB, and +44 dBm OIP3 (Mini-Circuits ZHL-10M4G21W0+).

## 2 Measurements

We characterized our OFO by measuring its performance at shift frequencies spaced by 20 MHz over the operational range of the sawtooth generator and spectrum analyzer. At each frequency we vary the amplitude of the waveform until optical power in the first sideband is maximized. We then measure the amplitude of the carrier, the first sideband, and the most prominent spurious feature. Then, with RF off, we measure the carrier. This is repeated 5 times for each frequency and the average performance is recorded. We observed that the PER of the fiber link that transmits laser light to the EOM drifts by  $\pm 2.6$  dB over an hour, so we frequently check the PER and adjust the paddles upstream of the EOM as necessary. Ultimately, PER limits the maximum contrast of our measurements to 26 dB.

Our observations for  $N = 1$  are in Figure 1. A conversion loss of  $< 1$  dB was maintained over 40 – 550 MHz,  $< 2$  dB over 40 – 1330 MHz and a suppression of  $> 10$  dB maintained over 40 – 1490 MHz. The lowest conversion loss was 0.095(20) dB at 40 MHz and the highest suppression was 24.72(28) dB at 100 MHz (reported error is statistical).. The broadband conversion loss was smoothly-varying, while suppression showed greater irregularities (Figure 1).

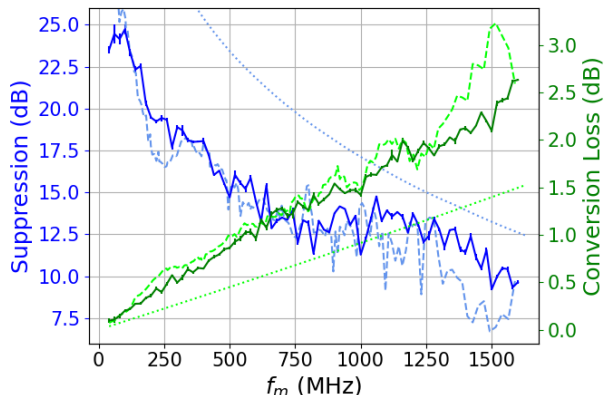


Figure 1: OFO performance for  $N = 1$  as a function of the modulation frequency. The dotted lines show predicted performance for a DAC with finite sampling frequency  $f_s = 9.85$  GSPS. The dashed lines extend this model to include the measured DAC-to-optical transfer function  $T_{\text{DTO}}$ .

To better understand our observations we explored two models. The first was to gauge the impact of finite AWG sampling frequency  $f_s$  on the sawtooth ramp. This model samples an ideal sawtooth wave of frequency  $f_m$  at a sampling rate  $f_s$  and interpolates between these samples to produce the modula-

tion waveform. We assume the DAC analog front end permits full-scale voltage swings in the interval  $1/f_s$ . To achieve a conversion loss  $< 1$  dB or suppression  $> 15$  dB,  $f_m/f_s < 0.11$  is required. It's clear from measured performance that finite AWG sampling frequency didn't limit our OFO (Fig. 1).

Next we considered the contribution of RF pipeline imperfections. We used a 50 GSPS oscilloscope (Tektronix DSA72004B) to characterize the transfer function of the amplifier. We combined this with manufacturer's factory test data for the EOM to estimate the overall DAC-to-optical transfer function  $T_{\text{DTO}}$  (shown in Figure 2), which maps the signal present at the DAC output (in the frequency domain) to the induced phase modulation at the EOM (in the frequency domain). We then numerically calculate the RF-pipeline-limited OFO performance. Let  $\mathbf{S}$  be a computer-generated sampling-frequency-limited sawtooth waveform with unit amplitude, ramp frequency  $f_m$ , and sample frequency  $f_s = 9.85$  GSPS. Writing the E-field of the modulated light in phasor notation and isolating its dependence on the phase modulation, we can extract the expected performance from the spectrum

$$\mathcal{F}\{\exp(ia\Phi)\} \quad (2)$$

where

$$\Phi = \mathcal{F}^{-1}\{T_{\text{DTO}}\{\mathcal{F}\{\mathbf{S}\}\}\}$$

and  $\mathcal{F}$  denotes the numerical fast Fourier transform. The value  $a$  (modulation amplitude) is varied until the predicted conversion loss is minimized; performance at this amplitude is then recorded. Repeating this procedure for various  $f_m \in [40, 1600]$  MHz produces the dashed lines in Figure 1. We find good agreement with measured performance. This suggests that predistorting the AWG waveform would improve performance.

A prospective way to improve performance for a given DAC frequency is to increase  $N$  (Eq. 1). Low  $V_\pi$  is advantageous as the maximum value of  $N$  is ultimately limited by the EOM maximum power. Here, it limits us to  $N < 5$ . We measured performance for our setup at these higher shift indices (Figure 3). We found no significant gains in performance. We checked for change in the DAC-amplifier transfer function at higher output power but did not see notable change. Furthermore, the curves shown here match simulations of the RF pipeline performance at higher modulation amplitudes (Figure 4). This is further support that performance is limited by imperfections in the DAC-to-EOM RF pipeline.

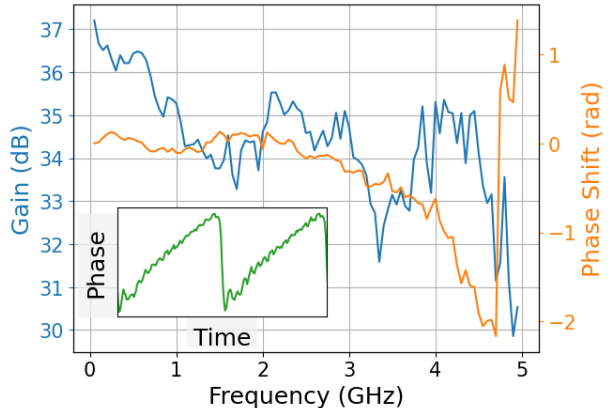


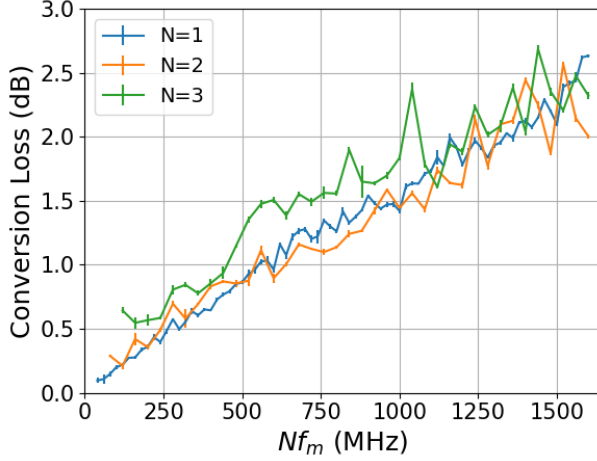
Figure 2: Measured DAC-to-optical transfer function  $T_{\text{DTO}}$ . To illustrate the effect of this nonuniform transfer function, the plot in the bottom left shows the resulting phase modulation for a sampling-frequency-limited input saw wave at 300 MHz.

### 3 Application to PDH Offset Locking

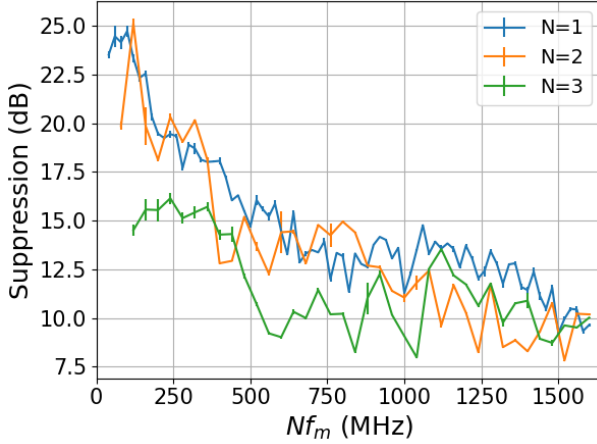
In this section we discuss in detail an application where a high-bandwidth OFO with strong spur suppression is of particular value. Namely, locking a laser to an optical cavity using the PDH technique with a continuously-tunable offset frequency. Concern about spurious PDH error signals due to unwanted features in the optical spectrum probing the cavity are an acknowledged problem and several modulation schemes have been developed to mitigate this issue [4, 19, 20, 21], however there is no published analysis quantifying the magnitude of the spurious error signal resulting from probing a cavity with an imperfectly coupled laser beam. In practice such technical imperfections are inevitable in laboratory setups; we remedy this gap as further motivation for OFO with strong spur suppression.

We propose two new metrics to evaluate offset locking performance. The first metric considers laser frequency error due to imperfect cavity mode matching and unwanted spectral features in the offset laser spectrum. The second metric is the offset frequency dynamic range. We discuss the consequences of each for PDH locking, then we demonstrate continuous tuning of a spectroscopy laser by 1.5 GHz. For clarity, we denote optical cavity mode frequencies with  $\nu_{\dots}$  (in Hz) and spectral features of the laser beam used for offset locking with  $\xi$  (in Hz).

Fabry-Pérot optical cavities are widely used as ultra-stable references for laser-frequency stabilization and linewidth narrowing. Ideally, the in-



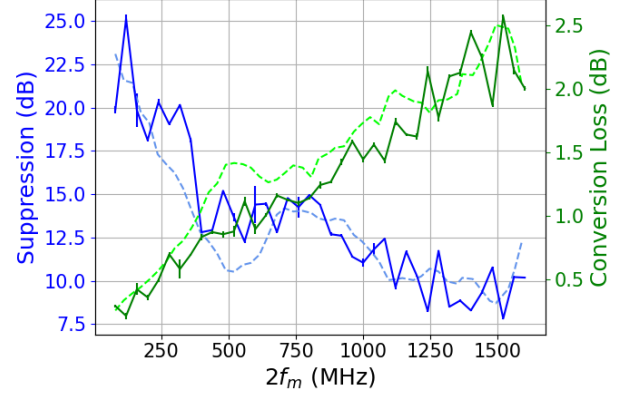
(a) Conversion loss for various  $N$ .



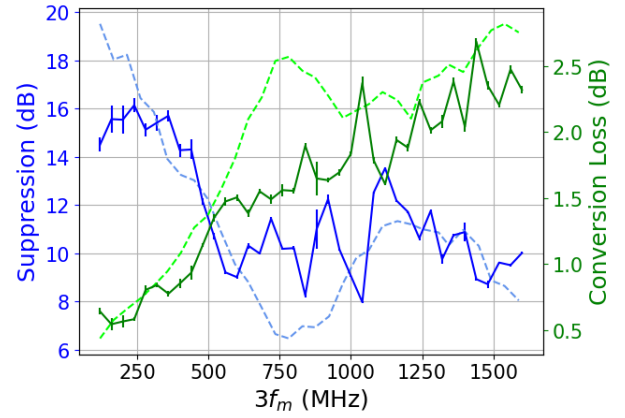
(b) Suppression for various  $N$ .

Figure 3: RFSoc performance for shift indices  $N = 1, 2, 3$  as a function of the imparted frequency shift  $Nf_m$

put Gaussian laser beam would be properly mode-matched to excite only the cavity's fundamental transverse mode  $\text{TEM}_{00}$ ; however, tip-tilt and transverse displacement misalignments permit excitation of higher-order Hermite-Gaussian modes  $\text{HG}_{mn}$  ( $m, n \in \{\mathbb{Z} > 0\}$ ). Furthermore, incorrect incident beam waist size or waist axial position permit excitation of Laguerre-Gaussian modes  $\text{LG}_{pl}$  ( $l, p \in \{\mathbb{Z} > 0\}$ ;  $p$  enumerates radial mode order,  $l$  enumerates angular mode order) [22]. These higher-order modes appear on the positive side of the fundamental mode at  $\nu_{00} + k\nu_h$ , where  $k = m + n$  for  $\text{HG}_{mn}$  mode,  $k = 2p + l$  for  $\text{LG}_{pl}$  modes and  $\nu_{00}$  is a  $\text{TEM}_{00}$  mode frequency. The frequency  $\nu_h$  only depends on cavity geometry



(a) Performance for  $N = 2$



(b) Performance for  $N = 3$

Figure 4: RFSoc performance for shift indices  $N = 2, 3$  as a function of the imparted frequency shift  $Nf_m$ . The dashed lines represent predicted performance for a 9.85 GSPS DAC with DAC-to-optical transfer function  $T_{\text{DTC}}$ .

$$\nu_h = \frac{1}{\pi} \nu_{\text{FSR}} \arccos \left[ \sqrt{\left(1 - \frac{d}{R_1}\right) \left(1 - \frac{d}{R_2}\right)} \right] \quad (3)$$

Here we assume a cavity of length  $d$ , spherical mirrors with radius of curvature  $R_1, R_2$  and free spectral range  $\nu_{\text{FSR}} = c/2d$ . Consider the lowest-order modes that emerge in the event of misalignment:  $\text{HG}_{10}, \text{HG}_{01}$  at  $+\nu_h$  and  $\text{LG}_{10}$  at  $+2\nu_h$ . These higher-order resonances can be observed on the transmitted (or reflected) light when scanning the probe laser frequency. Let  $C_k = V_{00}/V_k$  be the alignment contrast where  $V_{00}$  is the photodetector (PD) signal for the  $\text{TEM}_{00}$  mode and  $V_k$  is the PD signal for the mode offset by  $k\nu_h$ . If a probe laser of frequency  $\xi$  is scanned across the cavity FSR, the transmitted PD

voltage signal has the spectrum:

$$\begin{aligned}
V_{\text{PD}}(\xi) = & V_{00} \sum_n L(\xi, n\nu_{\text{FSR}}) \\
& + \frac{1}{C_1} L(\xi, n\nu_{\text{FSR}} + \nu_h) \\
& + \frac{1}{C_2} L(\xi, n\nu_{\text{FSR}} + 2\nu_h)
\end{aligned} \quad (4)$$

where

$$L(x, x') = \frac{1}{1 + \left(\frac{x-x'}{\delta\nu_c/2}\right)^2}$$

is a Lorentzian lineshape with cavity FWHM linewidth  $\delta\nu_c$ . As an example, consider  $d = 100$  mm,  $R_1 = 500$  mm and  $R_2 = \infty$  so that  $\nu_{\text{FSR}} = 1.5$  GHz and  $\nu_h = 0.221$  GHz. We observe that when  $C_1 \sim 30$  and  $C_2 \sim 15$  (typical for our 870 nm laser-cavity system), laser-cavity alignment is stable for more than a week at a time. Better alignment is possible but requires more frequent adjustment. In practice, transverse-position and angular-tilt misalignment are easier to reduce, while beam waist size and waist axial position are harder; typically  $C_1 > C_2$ . Figure 5(a) shows an example of a misaligned cavity spectrum.

Here we show how an undesired spectral feature in the offset laser that overlaps with a misaligned cavity mode can cause a spurious frequency shift in a PDH-locked laser (Fig. 5(b)). For an idealized PDH lock, a small frequency deviation  $\Delta\xi \ll \delta\nu_c/2$  in the offset laser beam with power  $P_{00}$ , generate an error signal with zero time average  $\langle V_{\text{err}} \rangle = 0$  [23]: that is, the laser is locked. If a spur with power  $P'$  overlaps with a higher-order cavity mode near  $\nu_{00} + k\nu_h$ , we get a spurious error signal voltage  $V_{\text{spur}}$  (see Fig. 5). If the spur is at  $\nu_{00} + k\nu_h - \delta\nu_c/2$  the error is maximal

$$V_{\text{spur}}^{\text{max}} = k'_e \frac{\delta\nu_c}{2} \quad (5)$$

where the error-signal slope at the higher order cavity mode is  $k'_e \propto P'/C_k$ . Since the PD output is a sum of the desired and spurious signals, the shift in the lock point due to  $V_{\text{spur}}^{\text{max}}$  is

$$\Delta\xi_{\text{spur}}^{\text{max}} = V_{\text{spur}}^{\text{max}}/k_e = \frac{1}{C_k} \frac{P'}{P_{00}} \frac{\delta\nu_c}{2} \quad (6)$$

Assuming cavity linewidth  $\delta\nu_c = 200$  kHz,  $P'/P_{00} = 1/10$ , and  $C_k = 10$ , we get  $\Delta\xi_{\text{spur}}^{\text{max}} = -1$  kHz. If the offset laser light were instead obtained from simple sinusoidal modulation (“DSB” scheme in [4]), the optical power is maximal (and equal) in the  $\pm 1$  sidebands for a modulation depth  $\approx 1.84$  rad. In the DSB case if the laser is locked to the +1 feature, the worst-case interaction of the -1 feature ( $P'/P_{00} = 1$ ) with

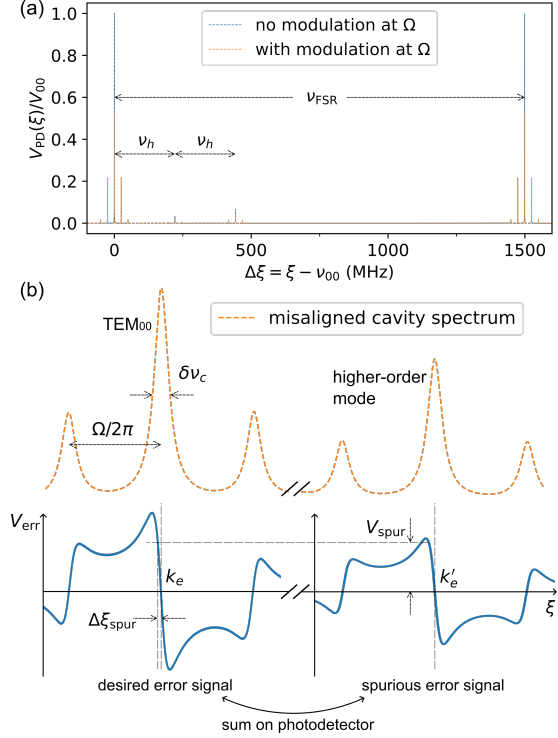


Figure 5: This figure illustrates our first metric: the frequency in a PDH-locked laser due to the interplay between imperfect cavity mode matching and unwanted spectral features in the offset laser spectrum. (a) Illustration of PD signal for light transmitted by a misaligned cavity (Eq. 4). The horizontal axis is the incident-laser detuning relative to a TEM<sub>00</sub> cavity mode at  $\nu_{00}$ . Here we assume a cavity with  $d = 100$  mm,  $R_1 = 500$  mm,  $R_2 = \infty$ ,  $\delta\nu_c = 200$  kHz,  $C_1 = 30$ ,  $C_2 = 15$  and  $C_k = 0$  for  $k > 2$ . The orange (blue) lines show the transmitted PD spectrum with (without) PDH phase modulation at  $\Omega/2\pi = 25$  MHz and depth  $\beta = 1.082$  rad where the PDH error signal slope  $k_e$  (V/Hz) is maximized. (b) Illustration of the mechanism underlying a shift in the PDH locking point. The left-hand (right-hand) side shows a zoom-in around  $\Delta\xi = 0$  ( $\Delta\xi = \nu_h$ ); the upper orange trace is the PD signal and the lower blue trace is the resulting PDH error signal with slope  $k_e$  ( $k'_e$ ). Ideally, the laser is locked to the left-hand feature so that  $V_{\text{err}} = 0$  and the right-hand feature is absent. The dashed horizontal line marks the spurious PDH error signal due to laser light near the higher-order mode at  $\nu_h$  which gives rise to an offset  $V_{\text{spur}}$  in the PDH error signal and a corresponding spurious lock point shift  $\Delta\xi_{\text{spur}} = V_{\text{spur}}/k_e$ . Note that  $\delta\nu_c$ ,  $\Omega/2\pi$ , and the contrasts for this figure are exaggerated to articulate certain effects. Physically realistic parameters are used in the calculation in Figure 6

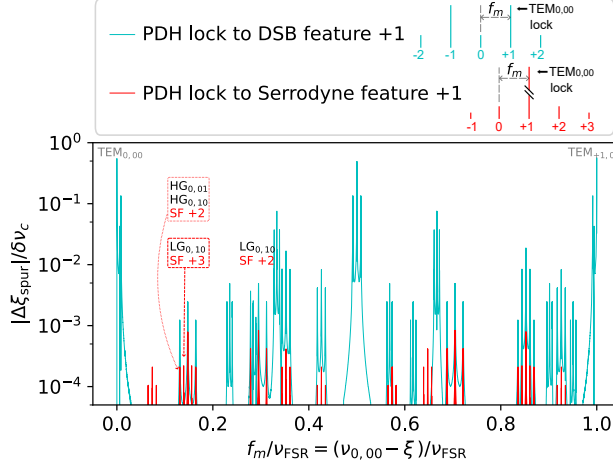


Figure 6: Here we plot the shift in a PDH-locked laser due to interaction of the HG<sub>01</sub>, HG<sub>10</sub> and LG<sub>10</sub> cavity modes with unwanted spectral features of the EOM-offset laser light. Here we assume a cavity with  $d = 100$  mm,  $R_1 = 500$  mm,  $R_2 = \infty$ ,  $\delta\nu_c = 200$  kHz,  $\Omega/2\pi = 25$  MHz,  $C_1 = 30$ ,  $C_2 = 15$  and  $C_k = 0$  for  $k > 2$ .  $f_m$  is DSB or serrodyne EOM modulation frequency.  $f_m = \nu_{0,00} - \xi$  for an offset lock to a TEM<sub>0,00</sub> mode. (DSB+1) The blue trace corresponds to single-tone drive of the EOM with depth  $\beta \approx 1.84$  rad and PDH locking the TEM<sub>0,00</sub> cavity mode to the upper (+1) optical sideband. The calculation includes the 0,  $\pm 1$ ,  $\pm 2$  spectral features emitted by the EOM. (Serrodyne+1) The orange trace corresponds to serrodyne drive of the EOM and PDH locking the TEM<sub>0,00</sub> cavity mode to the +1 feature. The calculation includes the 0,  $\pm 1$ , +2 and +3 serrodyne features (SF). The relative peak heights follow those observed experimentally: relative to the +1 feature, 0, +2 are 13 dB lower and  $-1$ , +3 are 16 dB lower. Here we distinguish cavity modes in different FSR ranges by adding a new index  $q$  (e.g., TEM <sub>$q$ ,00</sub>) because spurious features will interact with modes spanning multiple FSR. The vertical axis shows the relative lock point shift (see Fig. 5(b)). As an example,  $\Delta\xi_{\text{spur}}$  around  $f_m = \nu_h$  arises due to the interplay between SFs and cavity modes indicated in the red dashed boxes. Note that  $\Delta\xi_{\text{spur}}$  is zero at some cavity modes because SF 0, +2 and  $-1$ , +3 are assumed to have equal contrasts and they cancel out, which is unlikely in practice.

a higher-order cavity mode gives  $\Delta\xi_{\text{spur}}^{\text{max}} = 10$  kHz; the 0 and  $\pm 2$  sidebands give 3 kHz shifts. To better compare the the serrodyne and DSB EOM modulation schemes, Figure 6 shows a calculation of the offset-frequency-dependent laser-lock shift for realistic parameters.

The second metric we propose is the offset-frequency dynamic range. Let the offset frequency  $f_m$  lie in the range  $f_1$  to  $f_2$ , where  $f_1 < f_2$ . For any given offset frequency, let  $P_{00}$  be the optical power interacting with the cavity TEM<sub>00</sub> mode. As the offset frequency increases, the optical power in  $P_{00}$  decreases causing a reduction in the PDH error signal slope  $k_e$ . When the error signal is used for laser locking, the open-loop transfer function  $\hat{\alpha} \propto k_e \propto P_{00}$  determines laser noise suppression and certain lock parameters including the unity-gain point. Notably, if  $P_{00}$  drops by 3 dB the phase margin is degraded by about 20° [24] which can compromise lock stability [25]. This suggests the maximum for  $f_2$  is when  $P_{00}(f_2)/P_{00}(f_1) = 1/2$ .

## 4 Conclusion

We used commodity optoelectronic components to produce continuous wideband ( $\sim 1$  GHz) optical frequency offsets (OFO) in CW lasers with  $> 10$  dB spur suppression,  $< 2$  dB conversion loss and smoothly varying gain (Fig.1). Relative to other demonstrations we improve on simultaneous optimization of these parameters (Table 1). A simple model accounting for DAC-to-optical transfer function imperfections predicts observed performance. We compared serrodyne modulation (SM) with ordinary dual-sideband (DSB) modulation in a practical context: a PDH offset lock that is continuously swept with laser-cavity misalignment. For DSB modulation, the  $-1$  spur can give rise to unwanted laser frequency shifts of  $\sim \delta\nu_c/10$  for a misaligned cavity contrast of 5. While for SM modulation where all spurs lie below  $-13$  dB, the maximum unwanted shift is  $< \delta\nu_c/1000$ .

Going forward, as the cost of high-bandwidth DACs continues to decrease, we anticipate that high-

Source	OFO Method	Shift range (MHz)	< 1dB conversion loss (MHz)	< 2dB conversion loss (MHz)	> 10dB suppression (MHz)
[15]	SM via NLTL & EOM	100-1650	1490-1500	960-1070	X
[13]	coherent waveguide coupling (OC)	8000-11,000	8140-11,000	8000-11,000	X
[16]	SM via NLTL & EOM	200-1600	500-530	670-1240	940-1200
[26]	SM via NLTL & EOM	50-750	X	610-640	600-650
this manuscript	SM via AWG & EOM	40-1600	40-550	40-1330	40-1490

Table 1: Comparison of OFO methods for CW light with an emphasis on high bandwidth and spurious signal suppression. SM denotes serrodyne modulation, NLTL denotes nonlinear transmission line, OC denotes on-chip, and X indicates unreported data. The columns include the widest frequency range over which OFO demonstrations exhibited a particular level of conversion or suppression. Some demonstrations discussed in this paper are not included due to lack of broadband ( $> 100$  MHz) testing. Relative to prior work, we improve on spur suppression bandwidth by a factor of 5.

bandwidth, high-suppression OFO will emerge as a routine tool. A natural next step is to apply predistortion to the waveform using a true arbitrary waveform generator. The laser frequency errors modeled in Section 3 could be measured experimentally with access to a laser frequency comb or secondary cavity-locked laser.

## 5 References

- [1] T. Kawanishi, T. Sakamoto, and M. Izutsu, *IEEE Journal of Selected Topics in Quantum Electronics* **13**, 79 (2007).
- [2] J. L. Hall and T. W. Hänsch, *Opt. Lett.* **9**, 502 (1984).
- [3] J. L. Hall, L. Hollberg, T. Baer, and H. G. Robinson, *Applied Physics Letters* **39**, 680 (1981).
- [4] J. I. Thorpe, K. Numata, and J. Livas, *Opt. Express* **16**, 15980 (2008).
- [5] D. Zhu et al., *Light Sci Appl* **11**, 327 (2022).
- [6] D. Uttam and B. Culshaw, *J. Lightwave Technol.* **3**, 971 (1985).
- [7] R. I. MacDonald, *Appl. Opt.* **20**, 1840 (1981).
- [8] E. A. Donley, T. P. Heavner, F. Levi, M. O. Tataw, and S. R. Jefferts, *Review of Scientific Instruments* **76**, 063112 (2005).
- [9] C. Zhou et al., *Review of Scientific Instruments* **91**, 033201 (2020).
- [10] QUBIG GmbH, *Free-Space Phase Modulators*, WWW document, (<https://www.qubig.com/>).
- [11] A. Kodigala et al., *Sci. Adv.* **10**, eade4454 (2024).
- [12] H.-P. Lo and H. Takesue, *Optica*, *OPTICA* **4**, 919 (2017).
- [13] Y. Hu et al., *Nature* **599**, 587 (2021).
- [14] L. Johnson and C. Cox, *J. Lightwave Technol.* **6**, 109 (1988).
- [15] R. Houtz, C. Chan, and H. Müller, *Opt. Express* **17**, 19235 (2009).
- [16] D. M. S. Johnson, J. M. Hogan, S.-w. Chiow, and M. A. Kasevich, *Opt. Lett.* **35**, 745 (2010).
- [17] K. F. Lee and G. S. Kanter, *Opt. Express* **29**, 26608 (2021).
- [18] M. Kim et al., *Opt. Lett.* **45**, 6555 (2020).
- [19] J. Bai, J. Wang, J. He, and J. Wang, *Journal of Optics* **19**, 045501 (2017).
- [20] T. Rabga et al., *Optics Express* **31**, 41326 (2023).
- [21] J. Tu et al., *Quadrature amplitude modulation for electronic side and Pound-Drever-Hall locking*, 2024.
- [22] D. Z. Anderson, *Appl. Opt.* **23**, 2944 (1984).
- [23] E. D. Black, *American Journal of Physics* **69**, 79 (2001).
- [24] W. C. Wang, TBD (2024).
- [25] K. Ogata, *Modern control engineering*, Prentice-Hall electrical engineering series. Instrumentation and controls series, Prentice-Hall, Boston, 5th ed edition, 2010.

[26] M. Barbiero et al., *Opt. Lett.* **48**, 1958 (2023).